Industrial Crops & Products 230 (2025) 121102

Contents lists available at ScienceDirect

Industrial Crops & Products

journal homepage: www.elsevier.com/locate/indcrop

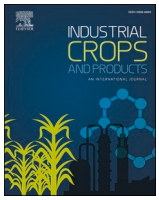

# Construction of Zn-based metal–organic frameworks in bamboo by in-situ and ex-situ growth strategies for indoor environmental remediation

Dujuan Wu [a,1], Ruiqi Xin [a,1], Lingling Hu [a,*], Onder Tor [c], Ye Song [a], Song Li [a], Meiling Chen [b,*], Wenkai Zhu [a,*]

[a] College of Chemistry and Materials Engineering, Zhejiang A&F University, Hangzhou 311300, China
[b] Co-Innovation Center of Efficient Processing and Utilization of Forest Resources, College of Materials Science and Engineering, Nanjing Forestry University, Nanjing 210037, China
[c] Department of Forest Industry Engineering, Kastamonu University, Kastamonu 37150, Turkey

ARTICLE INFO

*Keywords:*
Metal–organic frameworks
Delignified bamboo
Formaldehyde adsorption
Indoor environmental remediation

ABSTRACT

Indoor air pollution presents a significant challenge to human health, driving the development of advanced materials for indoor environmental remediation. Metal–organic frameworks (MOFs) derived materials possess great promise as promising candidates for addressing this challenge. In this work, the delignified bamboo with multi-scale structure was employed as a substrate to fabricate ZIF-8@bamboo by in-situ and ex-situ growth strategies. The results demonstrated that the delignified bamboo exposed polysaccharided cellulose active group originally present in the bamboo cell walls. The pretreated bamboo was facilitated to the uniform growth of ZIF-8 crystals, and the loaded ZIF-8 exhibited high crystallinity and well-distributed morphological characteristics. Moreover, the successful growth of ZIF-8 increased the bamboo's specific surface area. Additionally, the formaldehyde adsorption tests revealed that the ZIF-8@bamboo exhibited a 227.73 % improvement for formaldehyde adsorption rate at room temperature. Meanwhile, it also showed a rapid adsorption rate, high adsorption capacity, and reusable performance for formaldehyde. Furthermore, the as-prepared ZIF-8@bamboo demonstrated high removal efficacy for other indoor pollutants, including PM2.5 and PM10. Moreover, the ZIF-8@bamboo exhibited high indoor pollutant removal efficiency after five repeated cycles. Therefore, the ZIF-8@bamboo proposed in this work provides an effective solution to address indoor environmental pollution.

## 1. Introduction

In contemporary life, people spend over 90 % of their time indoors, where air pollutant concentrations are typically two to five times higher than outdoors (Dimitroulopoulou et al., 2023; González-Martín et al., 2021). Indoor pollutants like formaldehyde, benzene, and fine particulate matter (PM2.5, PM10) can directly threaten human health, causing non-specific symptoms with short-term exposure and exacerbating respiratory diseases, skin conditions, neurological disorders, and increasing cancer risks with prolonged exposure (Xin et al., 2024). Therefore, removing indoor pollutants is crucial for public health improvement.

Several strategies mitigate indoor air pollution, including physical adsorption, chemical decomposition, and activated carbon adsorption (Robertson et al., 2024; Tran et al., 2020; Wang et al., 2024). In materials science, nanomaterials like quantum dots, metal oxides, carbon nanotubes, graphene, and metal–organic frameworks (MOFs) are applied for indoor environmental remediation due to their porous properties and high specific surface areas (Chen et al., 2021; Ahmad et al., 2023; Haghighi and Haghighat, 2024; Wang et al., 2024). Among these, MOFs show significant potential for indoor air pollutant removal due to their extremely high specific surface area and tunable pore characteristics (Wang et al., 2019). They possess large adsorption capacities and can enhance specific pollutant removal by altering chemical composition (Safaei et al., 2019). Zeolitic imidazolate frameworks (ZIFs), a subclass of MOFs composed of cationic transition metal ions and imidazole ligands, exhibit zeolite-like topology and unique properties (Kouser et al., 2022). ZIFs' structure, similar to silica aluminate zeolite, offers adjustable pore size and structure, showing great flexibility in various applications. Their structure and properties can be modulated by selecting different metal ions and organic ligands to adapt

* Corresponding authors.
*E-mail addresses:* linglinghu@zafu.edu.cn (L. Hu), meiling1226@163.com (M. Chen), wenkai0814@zafu.edu.cn (W. Zhu).
[1] These authors contributed equally to this work.

https://doi.org/10.1016/j.indcrop.2025.121102
Received 18 January 2025; Received in revised form 14 April 2025; Accepted 24 April 2025
Available online 5 May 2025

to indoor pollutant removal (Guo et al., 2022; Wang et al., 2024d).

ZIFs have shown outstanding performance in many fields, such as gas storage, adsorption separation, and drug delivery (Denning et al., 2021; Sun et al., 2012). They exhibit superior thermal and chemical stability compared to other MOFs, especially ZIF-8. ZIF-8 is highly practical due to straightforward synthesis, mild conditions, and easy crystal formation (Nazir et al., 2025). Its exceptional stability retains structure even after extended liquid immersion (Butt et al., 2023). ZIF-8's unique advantages show excellent adsorption performance for gaseous pollutants and high promise for pollutant removal (Zhu et al., 2022). However, ZIF-8's crystalline effect and tendency to agglomerate result in poor processability and weak recyclability (Elaouni et al., 2022). Constructing composites by integrating ZIF-8 with a substrate addresses these issues.

Suitable substrates for combining with ZIF-8 include inorganic materials, polymers, and biomass materials (He et al., 2024; Cao et al., 2024; Zhang et al., 2021; Shi et al., 2024). Among these, bamboo stands out due to rapid growth, lightweight, high strength, and tensile properties (Hu et al., 2024; Feng et al., 2024), providing an excellent structural base for MOF crystal growth. Bamboo's flexibility, ease of processing, and unique micro-nano porous structure benefit macroarchitecture construction (Chen et al., 2024a; Othman et al., 2024). Meanwhile, Chemical treatments can enrich active groups on bamboo surfaces (like hydroxyl and carboxyl groups), facilitating interactions with nanomaterials (Liu et al., 2024). Leveraging bamboo's structural properties to support ZIF-8 overcomes mechanical strength limitations while conferring ZIF-8's adsorption performance. Consequently, developing a novel bamboo-based Zn-MOF macroarchitecture for indoor pollutant adsorption and storage is urgently needed.

To our best knowledge, the in-situ and ex-situ strategy are two common techniques for preparing MOFs-based macrostructures (Li et al., 2024b). The in-situ method can provide more uniform dispersion and stronger interfacial bonding, while the ex-situ method allowed for more precise control over the size and distribution of ZIF-8 crystals (Kharwar et al., 2022). In terms of production costs, the in-situ method is operationally simple and minimizes losses during transfer. The ex-situ method, while more complex, can be optimized for higher efficiency in large-scale production. Comparative analysis of these methods contributes to the development of more efficient material synthesis strategies (Jambovane et al., 2016). In this work, we combined bamboo's natural porous structure and fibrous characteristics with ZIF-8 to fabricate ZIF-8@bamboo via in-situ and ex-situ methods, achieving adsorption of common indoor pollutants.

## 2. Experimental

### 2.1. Materials

Four-year-old original-colored bamboo (*Phyllostachys edulis*) was prepared in Nanping, Fujian Province, China. Zinc acetate dihydrate ($C_4H_6O_4Zn{\cdot}2\ H_2O$), 2-methylimidazole ($C_4H_6N_2$, 2-MIM), methanol solution ($CH_3OH$), anhydrous ethanol ($C_2H_5OH$), and deionized water were provided by Shanghai Aladdin Biochemical Technology Co., Ltd. Sodium hydroxide (NaOH, 10 wt%) solution was purchased from Denzhou Xijing Biotechnology Co., Ltd. Unless otherwise specified, all reagents and solvents used in the experiments were not further purified. The delignified bamboo used throughout the experiments was pretreated with alkali, and the specific treatment process is described in Text. S1. In addition, the ZIF-8 used in the experiments was prepared with modifications by the previous method of our group (Zhu et al., 2023b), and the detailed preparation method is depicted in Text. S2.

### 2.2. In-situ growth strategy for preparing ZIF-8@bamboo

The schematic diagram for the construction of ZIF-8@bamboo by the

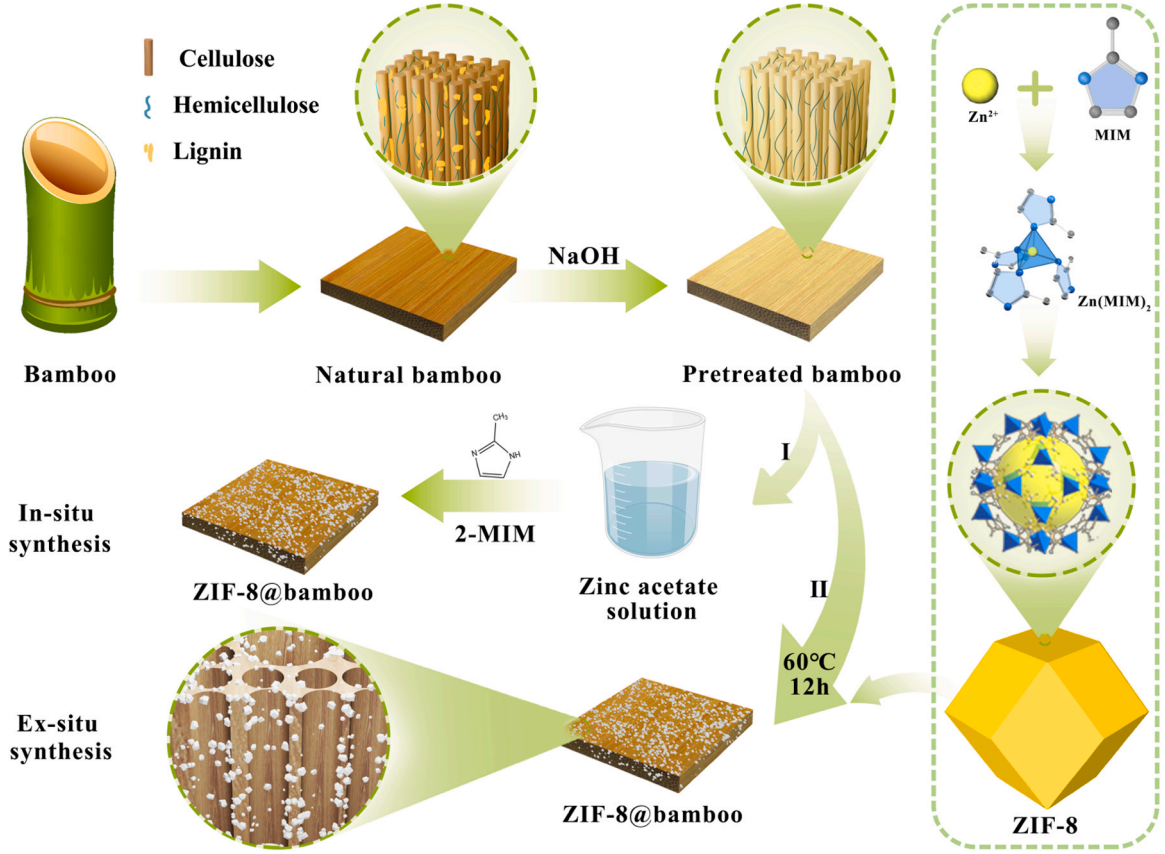


**Fig. 1.** Schematic illustration of the preparation of the ZIF-8@bamboo by in-situ and ex-situ growth strategies.

in-situ growth strategy is shown in Fig. 1-I. Firstly, $C_4H_6O_4Zn{\cdot}2\ H_2O$ (1.5 g, 3.0 g, and 4.5 g) was dissolved in 50 mL of methanol solution (95 wt%), and then stirred until homogeneous. The delignified bamboo was added to the solution and stirred for 5 hours at 200 rpm (Wang et al., 2024e). Next, 2-methylimidazole (4.488 g, 8.976 g, and 13.464 g) was mixed with 50 mL of methanol solution (95 % wt%), and added to the previous solution, followed by continued stirring for 8 hours. Then, the as-prepared ZIF-8@bamboo was rinsed three times with deionized water and dried in a vacuum oven at 60 °C for 8 hours. The ZIF-8@bamboo obtained by in-situ growth strategy with various $Zn^{2+}$ were labeled IN-1, IN-2, and IN-3.

### 2.3. Ex-situ growth strategy for preparing ZIF-8@bamboo

The schematic diagram for the preparation of ZIF-8@bamboo by the ex-situ growth strategy is shown in Fig. 1-II. Briefly, the as-prepared ZIF-8 crystals (0.148 g, 0.296 g, and 0.444 g) were dissolved in 100 mL of methanol solution. Subsequently, the solution was subjected to ultrasound dispersion using an ultrasonic disperser (SB-120DT, SCIENTZ, China) for 2 hours, followed by stirring on a magnetic stirrer (DF-101S, XIUILAB, China) for 6 hours. Then, the delignified bamboo was immersed in the mixture and stirred at 200 rpm for 12 hours. Subsequently, the sample was rinsed three times with deionized water and vacuum dried at 60 °C for 8 h. Finally, the ZIF-8@bamboo sample by the ex-situ growth strategy was successfully prepared and labeled as EX-1, EX-2, and EX-3, respectively.

### 2.4. Characterization

The morphology and structure of the samples were investigated by a cold field emission scanning electron microscope (SEM, SU8010, Tokyo, Japan) with an operating current of 20 mA and voltage of 15 kV. Elemental analysis was performed using energy-dispersive X-ray spectroscopy (EDX, X-MAX, USA). $N_2$ adsorption/desorption isotherms were confirmed using a BELSORP MINI X instrument (MicrotracBEL, Japan) at 77 K. X-ray diffraction (XRD) tests were conducted using a D2 Phaser (Bruker AXS, Germany) with a Copper (Cu) Kα radiation at 40 kV and 30 mA with a scanning speed of 4° per minute. Fourier-transform infrared spectroscopy was measured using a Cary630 (FT-IR, Agilent Technologies Inc., USA) in the wavelength range of 4000 $cm^{-1}$ to 500 $cm^{-1}$. X-ray photoelectron spectroscopy (XPS) was investigated using a K-ALPHA spectrometer (Thermo Fisher Scientific, USA) with X-ray irradiation of the material surface within an energy range of 0–1200 eV.

## 3. Results and discussion

### 3.1. Fabrication mechanism of ZIF-8@bamboo

The delignified bamboo was underwent an alkaline pre-treatment process, which exposed active groups on surface and facilitating the growth of ZIF-8 nanocrystals. This process results in the successful fabrication of ZIF-8@bamboo, as shown in Fig. 2. Additionally, the surface of the delignified bamboo exhibited a significant number of hydroxyl groups, which played a crucial role in stabilizing the structure of ZIF-8@bamboo through weak non-covalent bonds (Liu et al., 2024). When using ex-situ strategy to prepare ZIF-8@bamboo, ZIF-8 was attached to the delignified bamboo cellulose through hydrogen bonding and van der Waals forces. Moreover, the subsequent tests demonstrated that the delignified pretreatment bamboo promoted significant growth of ZIF-8 crystals. The alkaline treatment disrupted the hydrogen bonds in bamboo cellulose at the microscopic level, exposing hydroxyl groups capable of covalently bonding with ZIF-8 (Wang et al., 2024d). Meanwhile, the increased surface roughness of alkali-treated bamboo provided more active sites, facilitating the efficient attachment of ZIF-8.

The precursor of ZIF-8, $Zn^{2+}$ initially interacted with hydroxyl groups in the delignified bamboo cellulose throughout the in-situ strategy. This interaction typically involved ion exchange or coordination bond

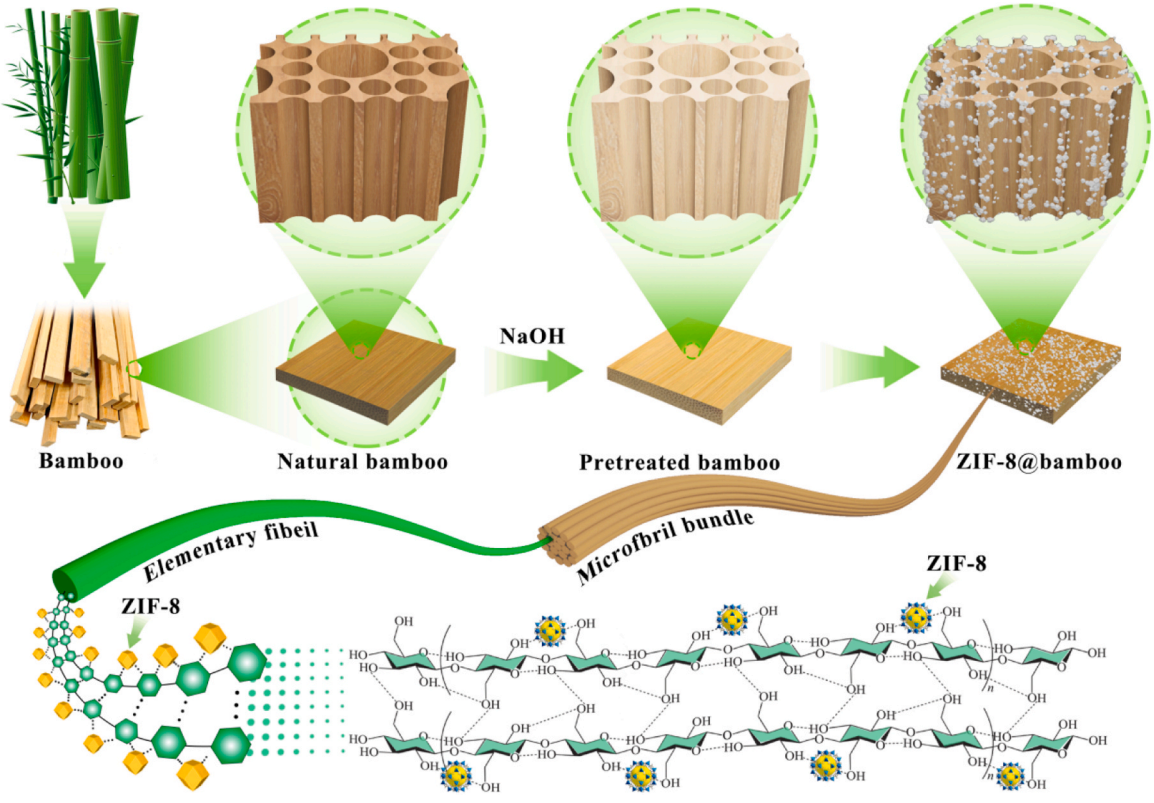


**Fig. 2.** Schematic mechanism of fabrication of ZIF-8@bamboo.

formation, providing a stable foundation for the subsequent nucleation of ZIF-8. Upon the introduction of 2-MIM into the reaction system, it formed a complex with the $Zn^{2+}$ bound to the exposed bamboo cellulose. The complexation process was facilitated by coordination bonds between the N of 2-MIM and $Zn^{2+}$, resulting in the direct formation of ZIF-8 nanocrystals on the surface of bamboo cellulose. Consequently, the abundant reactive hydroxyl groups on the bamboo surface after alkali pretreatment can interact with ZIF-8 precursor molecules via hydrogen bonding, thereby promoting the effective nucleation of ZIF-8. The advantage of in-situ strategy lied in ability to precisely control the size and morphology of ZIF-8 crystals, ensuring effective integration with the bamboo cellulose substrate.

### 3.2. Micromorphology and structure

The surface morphology, particle size, shape, and structural of the samples were investigated by using SEM, as shown in Fig. 3. The micromorphology of the as-prepared ZIF-8@bamboo by the ex-situ and in-situ methods is illustrated in Fig. 3a. Fig. 3c-d indicated that the ZIF-8 crystals synthesized via hydrothermal solvent methods exhibited a regular rhombic dodecahedral structure, consistent with the crystal morphology reported in the literature (Van Cleuvenbergen et al., 2018). Moreover, Fig. 3c revealed that the particle size of ZIF-8 crystals ranged from 500 to 1200 nm, with an average size of 858 nm (Fig. 3b). The particle size of ZIF-8 distribution appeared normal, indicating a relatively uniform size of the synthesized ZIF-8 crystals.

Fig. 3e shows that the surface of the as-prepared ZIF-8@bamboo was covered with a layer of crystalline material. According to Fig. 3f-h, both synthesis strategies successfully produced ZIF-8@bamboo and the in-situ growth method exhibited notably better results. Furthermore, the number of ZIF-8 particles combined in EX-1 was less than that in IN-1, and the uniformity of combining was slightly poorer. IN-1 demonstrates superior binding effectiveness. Furthermore, the as-prepared ZIF-8@bamboo through the ex-situ strategy showed that the ZIF-8 particle

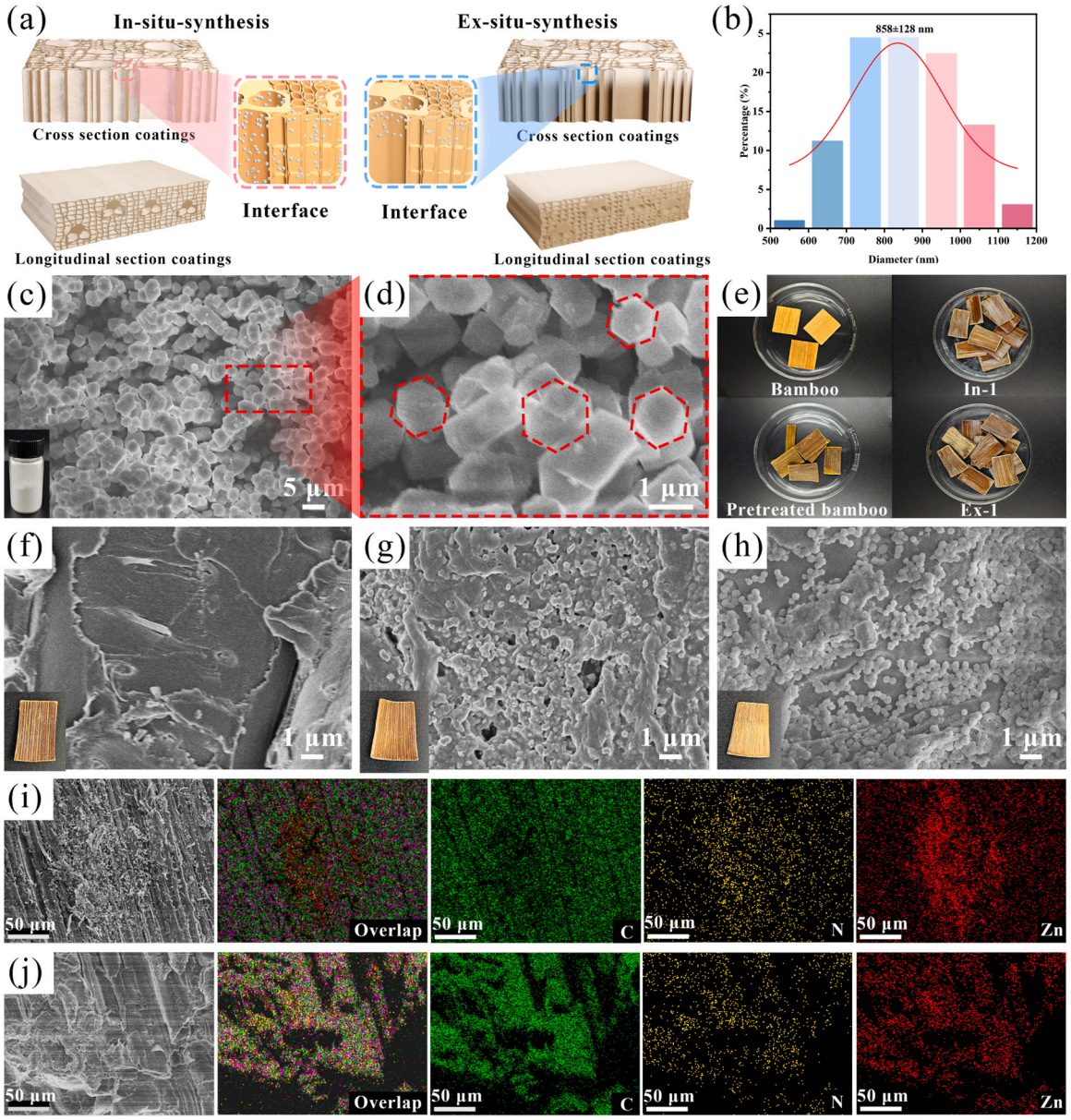


**Fig. 3.** (a) Schematic diagram comparing the effect of IN-1 and EX-1 combining. The particle size distribution (b) and SEM images (c,d) of as-prepared ZIF-8. (e) Optical photographs of the ZIF-8@bamboo samples. SEM images of ZIF-8@bamboo: M0 (f), EX-1 (g), IN-1 (h). EDS elemental mapping images of ZIF-8@bamboo: IN-1 (i), EX-1 (j).

size obtained at standard concentration was relatively small (Fig. S1a-c). The particle size of ZIF-8 grew and agglomeration became more pronounced with increased $Zn^{2+}$ concentration. This phenomenon was also observed in the SEM images by the in-situ growth method (Fig. S1d-f). Moreover, both Zn and N elements can be detected on the surface of the samples, and distributed uniformly (Fig. 3i-j). Therefore, the ZIF-8@bamboo prepared by in-situ strategy demonstrated superior performance in terms of both the quantity and uniformity of bonding.

### 3.3. Physical-chemical characterization

The composition, structure, and crystallinity of the ZIF-8@bamboo were characterized by XRD, FTIR, and $N_2$ adsorption-desorption, as depicted in Fig. 4a shows that the as-prepared ZIF-8 exhibited diffraction peaks consistent with those reported in the literature (Li et al., 2018), corresponding to (001), (002), (112), (022), (013), (222), (114), (233), (134), and (044). These characteristic peaks aligned with the simulated spectrum of ZIF-8, indicating that the as-prepared ZIF-8 had a pure, single-phase framework structure with high crystallinity and purity.

Furthermore, all the ZIF-8@bamboo samples displayed sharp and distinct diffraction peaks within the 0–40° range, which were the characteristic peaks of ZIF-8 (Fig. 4a). This observation confirmed that the as-prepared samples contained ZIF-8, which had high crystallinity and existed as a single pure phase. The diffraction peak observed at 22.4° was attributed to the (114) crystal plane of bamboo cellulose, exhibiting the characteristics of amorphous phases (Bao et al., 2024). This suggested that the ZIF-8 was successfully combined onto the bamboo surface without disrupting original structure.

FTIR spectrum was further investigated the chemical functional groups changes on the surface of ZIF-8@bamboo, as displayed in Fig. 4b. Stretching vibration absorption peaks at 3134 $cm^{-1}$ and 2932 $cm^{-1}$ correspond to the C-H bonds in the methyl and imidazole rings, respectively (Li et al., 2024a). The absorption peak at 1586 $cm^{-1}$ was attributed to the N-H bond in the imidazole ring. Additional stretching vibration peaks at 1145 $cm^{-1}$ and 993 $cm^{-1}$ correspond to C═N and C-N. Meanwhile, the sharp absorption peaks at 754 $cm^{-1}$ and 418 $cm^{-1}$ were arised from the bending vibrations of Zn-O and Zn-N (Cho et al., 2023). Notably, the Zn-N bond was a characteristic chemical bond of ZIF-8, indicating the bonding between Zn and N atoms. The presence of C═N and C-N stretching vibrations confirmed the existence of double bonds and N atoms in the synthesized metal-ligand molecules (Luo et al.,

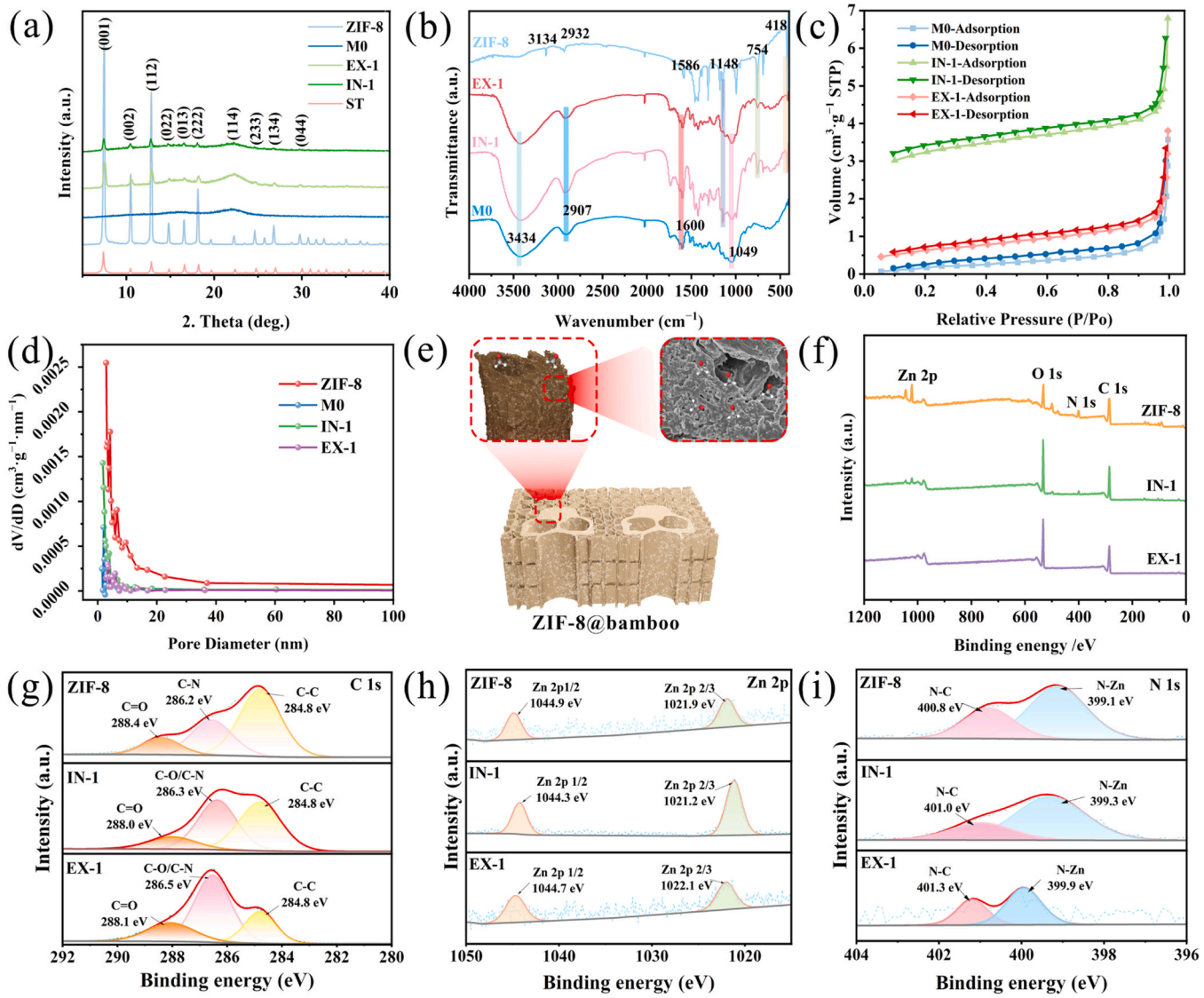


**Fig. 4.** Physical-chemical characterization of the ZIF-8@bamboo. XRD patterns (a), FTIR spectra (b), $N_2$ adsorption-desorption isotherms (c), and pore size distribution (d) of the ZIF-8@bamboo. (e) Schematic diagram of the porous structure of the ZIF-8@bamboo. The total survey XPS spectrum (f), and high resolution XPS spectra of C 1 s (g), Zn 2p (h) and N 1 s (i) of the as-prepared ZIF-8@bamboo.

2024; Sun et al., 2024b). A broad absorption peak at 3434 $cm^{-1}$ in Fig. 4b indicated the hydroxyl groups in bamboo, while the peak at 2907 $cm^{-1}$ arose from the C-H bonds in methyl. Multiple vibration absorption peaks between 1600 $cm^{-1}$ and 1049 $cm^{-1}$ correspond to C-O-C and C-C groups (Zhao et al., 2024). Comparing the M0 with the as-prepared ZIF-8, the results revealed distinct absorption peaks unique to each sample. The FTIR spectra of EX-1 and IN-1 showed the characteristic bamboo absorption peaks. The Zn-C vibration absorption peak appeared at 418 $cm^{-1}$ was a unique feature of ZIF-8. This result aligned with the XRD analysis, confirming the successful combining of $Zn^{2+}$ in the form of ZIF-8 onto the bamboo substrate.

The $N_2$ adsorption-desorption isotherms and micropore size distribution of the ZIF-8 exhibited a typical Type I isotherm without a hysteresis loop. Moreover, it gradually increases at low relative pressure and then reached saturation (Fig. S2). This indicated that ZIF-8 possessed a typical microporous structure without mesopores (Zhu et al., 2023a). The specific surface area of ZIF-8 was 844.7318 $m^2 \cdot g^{-1}$ , demonstrating exceptionally high surface area, which was determined by highly ordered porous structure. Additionally, the pore size of ZIF-8 was primarily distributed between 0 and 20 nm (Fig. 4d). These pore sizes suitable for adsorbing common indoor air pollutants, such as formaldehyde and PM2.5. The $N_2$ adsorption-desorption isotherms of M0 were Type II with a rapid increased in adsorption at low relative pressure. The adsorption reached a plateau but did not completely saturate at a relative pressure close to 1 (Fig. 4c). This indicated that the sample possesses a mesoporous structure, where adsorption and condensation within the pores coexist (Lee et al., 2024). Additionally, this suggested that the sample was suitable for applications in gas storage, catalyst carriers, and separation media. The pore structure of the sample fell within the microporous (2–50 nm) range according to the average pore size. The $N_2$ adsorption-desorption isotherms of IN-1 and EX-1 also showed that the samples fell within the microporous range (Fig. 4d). The specific surface area of the samples increased from 1.08 $m^2 \cdot g^{-1}$ (M0) to 11.58 $m^2 \cdot g^{-1}$ (IN-1) and 3.36 $m^2 \cdot g^{-1}$ (EX-1), indicating that the successful combining of ZIF-8 significantly enhanced the surface area of the bamboo (Table. S1). This hierarchical porous structure (Fig. 4e) and large surface area contributed to improve mass transfer rates and provided abundant active sites, thereby enhancing the efficiency of the ZIF-8@bamboo in removing indoor pollutants (Zhu et al., 2024).

### 3.4. Elemental analysis

Surface elemental analysis was conducted on the as-prepared ZIF-8@bamboo by in-situ and ex-situ methods. The EDS images clearly showed the presence of Zn and N elements, with a uniform distribution (Fig. 3i-j). XPS elemental content analysis revealed that the N content in ZIF-8@bamboo significantly increased compared to M0. The N content in IN-1 and EX-1 reached 2.57 % and 0.37 %, respectively (Table. S1). Concurrently, the C/N ratio in ZIF-8@bamboo had been enhanced to varying degrees (Table. S1). This phenomenon was attributed to the presence of N atoms in the 2-MIM of the ZIF-8 precursor (Qiu et al., 2024). The higher N content in the IN-1 sample suggested a greater amount of ZIF-8 binding, due to the uniform growth of ZIF-8 on the bamboo substrate during in-situ synthesis. In contrast, the lower N content in the EX-1 sample reflected a lower ZIF-8 combining, due to the uneven distribution of ZIF-8 particles on the bamboo substrate caused by the ex-situ strategy.

As shown in Fig. 4f, the sharp peaks corresponding to Zn 2p, C 1 s, O 1 s, and N 1 s were observed. The M0 did not exhibit N 1 s and Zn 2p peaks, indicating that the Z and N atoms from ZIF-8 were successfully incorporated into the bamboo. The high-resolution XPS spectrum of Zn 2p (Fig. 4h) showed the presence of Zn 2p 1/2 and Zn 2p 3/2 electron energies in both the in-situ and ex-situ combined bamboo substrates. During the in-situ synthesis, the bamboo substrate was thoroughly immersed in $C_4H_6O_4Zn \cdot 2\ H_2O$, leading to a significantly larger peak area for the IN-1 in the Zn 2p spectrum (Fig. 4h). Fig. 4g shows sharp peaks at 288.8 eV, 286.2 eV, and 284.8 eV represented C═O, C-N, and C-C bonds, respectively (Wang et al., 2024c; Xing et al., 2024). The peak height and area of the C-C decreased in both IN-1 and EX-1, indicating the presence of more C-O. The peaks at N 1 s spectrum represented N-C and N-Zn bonds (Fig. 4i). Since these bonds were absented in M0, the appearance in ZIF-8@bamboo once again confirmed the successful incorporation of ZIF-8. Furthermore, the shift of the peaks to the higher energy region suggested that amino groups participated in the reaction during the combining process, promoting the growth of ZIF-8. Additionally, the O 1 s spectrum shows peaks representing O-C and O═C bonds (Fig. S3). The samples M0, IN-1, and EX-1, due to prior bamboo pretreatment, experienced surface double bonds decreased. After being made into ZIF-8@bamboo, the ratio of O═C to O-C in the material is smaller. Thus, the graph shows a decrease in O═C and an increase in O-C. Meanwhile, the change in the chemical environment on the wood surface causes the oxygen bonds to shift towards a higher peak region (Yu et al., 2020).

### 3.5. Indoor pollutant removal performance

Formaldehyde serve as a major source of indoor pollution was evaluated by ZIF-8@bamboo using a self-made device (Fig. 5a). The detailed description of the formaldehyde adsorption testing procedure was displayed in the Text. S3. The formaldehyde adsorption efficiency (R) and adsorption amount ($Q_t$) were calculated by the following equations (Law et al., 2024; Wang et al., 2024g; Yen et al., 2024):

$$R = \frac{C_0 - C_t}{C_0} \times 100\% \quad (1)$$

$$Q_t = \frac{(C_0 - C_t) \times V}{m} \quad (2)$$

where $C_0$ represents the initial concentration of the pollutant, $C_t$ represents the final concentration of the pollutant, V is the volume of the apparatus, and m is the mass of the sample.

Meanwhile, the formaldehyde adsorption rate of as-prepared ZIF-8 was also evaluated (Fig. 5b). The formaldehyde concentration decreased significantly from 0.447 $mg/m^3$ to 0.211 $mg/m^3$ with the addition of ZIF-8, indicating a degradation rate was 52.80 % at this initial phase. Moreover, the formaldehyde concentrations stabilized at 0.156 $mg/m^3$ and 0.151 $mg/m^3$ after 7 h, respectively. This results suggested that the concentration of formaldehyde gas had nearly reached adsorption equilibrium. The data analysis revealed that 0.15 g ZIF-8 achieved a formaldehyde adsorption rate of 67.11 % and an adsorption amount of 0.296 $mg/m^3$ after 8 h. This data clearly demonstrated the excellent adsorption performance of ZIF-8 for formaldehyde.

Furthermore, the effect of various ZIF-8 contents and construction methods on the formaldehyde adsorption performance by the ZIF-8@bamboo was also explored. The formaldehyde concentration in the adsorption device was set at 0.40 $mg/m^3$ . The formaldehyde adsorption rate of M0 after 8 h was only 16.30 % (Fig. 5c). This indicated that the cellulose components in M0 had the capacity to remove formaldehyde, but the adsorption rate was low. However, the formaldehyde adsorption rate of the ZIF-8@bamboo improved significantly. Among them, the IN-2 exhibited the highest formaldehyde adsorption rate of 53.42 % (Fig. 5c), which was a 227.73 % increase compared to M0. Compared to $Cu_2O$ NPs@wood composite catalysts, our material shows higher formaldehyde adsorption efficiency and a simpler preparation process (Wang et al., 2024b). While commercial air purifiers with advanced photocatalytic filters like bimetallic Pt@Cu-$TiO_2$ demonstrate high formaldehyde removal efficiency, our material offers greater environmental benefits and sustainability (Bathla et al., 2023). Future optimizations in synthesis conditions could further lower production costs and enhance economic viability, making it a promising solution for air purification. Therefore, the ZIF-8@bamboo had an outstanding

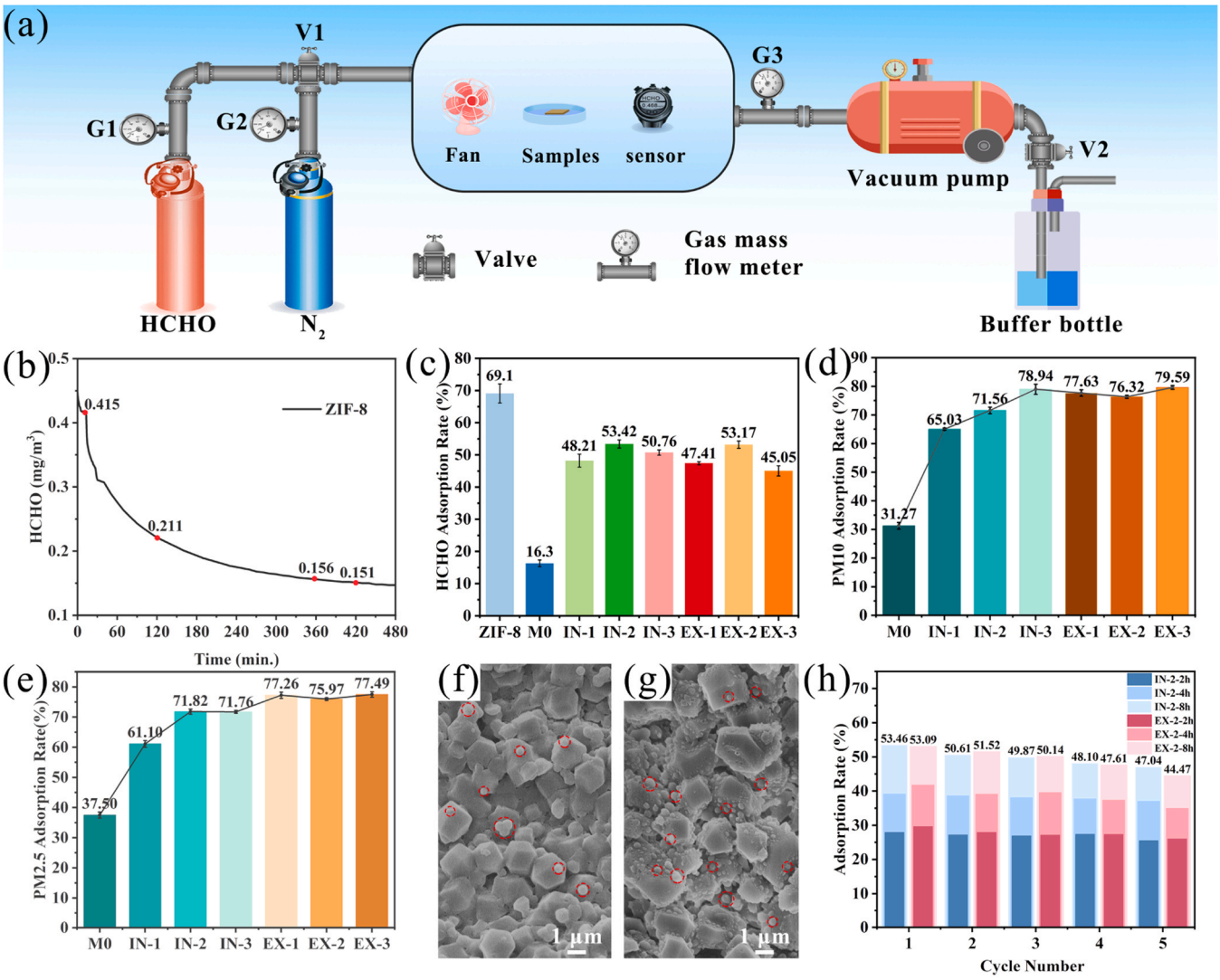


**Fig. 5.** (a) Schematic diagram of the self-made pollutant adsorption device. (b) Formaldehyde adsorption performance of 0.15 g ZIF-8. (c) Indoor formaldehyde adsorption rate of different samples. The adsorption efficiency of ZIF-8@bamboo for PM10 (d) and PM2.5 (e). SEM images of EX-2 (f) and IN-2 (g) after adsorption of indoor pollutants. (h) Reusability test of ZIF-8@bamboo on formaldehyde by five cycles.

performance for formaldehyde removal. The formaldehyde adsorption rates of the as-prepared ZIF-8@bamboo with increasing ZIF-8 concentrations followed a trend of increasing and then decreasing (Fig. 5c). This phenomenon was due to the high concentration of ZIF-8 crystals led to dense bonding with the bamboo cellulose, thus affecting the formaldehyde adsorption effect (Teng et al., 2024; Wang et al., 2024a). The formaldehyde adsorption rates of the EX samples were lower compared to the IN samples but still showed a significant improvement over M0. This could be attributed to the more uniform and deeper dispersion of ZIF-8 achieved with in-situ synthesis (Ye et al., 2024), which resulted in a larger surface area and superior formaldehyde adsorption performance. The adsorption rates of the ZIF-8@bamboo at varying concentrations displayed a trend of initially increasing and then decreasing rates (Fig. 5c). This phenomenon resulted from excessive ZIF-8 crystal content caused tighter packing of bamboo fibers, thus affecting formaldehyde adsorption. The ZIF-8@bamboo synthesized by ex-situ method showed lower formaldehyde adsorption rates than those by the in-situ method. Meanwhile, the ZIF-8@bamboo prepared by in-situ method showed more uniform dispersion, resulting in a greater specific surface area and enhanced formaldehyde adsorption performance.

The porous structure and large specific surface area of ZIF-8@bamboo suitable for adsorbing a variety of pollutants, offering broad application prospects in the field of indoor air purification. Furthermore, the ZIF-8@bamboo not only demonstrated excellent performance in formaldehyde removal but also effectively adsorbed other indoor pollutants. In this work, the ZIF-8@bamboo also showed outstanding performance in capturing inhalable particles such as PM2.5 and PM10, which was crucial for improving IAQ. The ZIF-8@bamboo exhibited significantly enhanced PM2.5 and PM10 adsorption capacity comparing with M0, with the adsorption rate generally more than doubling. The EX-3 showed superior adsorption properties for PM10 with an adsorption rate of 79.59 % (Fig. 5d). Meanwhile, the EX-3 sample also showed the highest adsorption rate for PM2.5 reaching 77.49 %, an increase of 111.97 % compared to M0 (Fig. 5e). This indicated that the incorporation of ZIF-8 significantly improved the ability of bamboo-based material to capture PM2.5. Overall, the adsorption efficiency of ZIF-8@bamboo for PM10 was generally higher than that for PM2.5. This phenomenon is due to the large particle size of PM10, which makes the material easier to capture.

Fig. 5f-g revealed that the surface of the ZIF-8 crystals remained intact, with the formation of small protruding structures following adsorption. Meanwhile, the recovered ZIF-8@bamboo retained structural integrity after the adsorption experiments. This contrasts with the unadsorbed samples (Fig. 3c), suggesting that the adsorption of

pollutant molecules altered the surface micromorphology. These microscopic structural changes confirmed the pivotal role of ZIF-8 crystals in the adsorption of indoor pollutants and underscore the enhanced adsorption performance of the ZIF-8@bamboo. This increased adsorption efficiency was attributed to the interactions between ZIF-8 crystals and pollutant molecules, effectively facilitating pollutant capture (Chen et al., 2024b; Shu et al., 2024).

### 3.6. Reusability and stability

The reuse of adsorbents is of great significance in practical applications (Baskar et al., 2022). As formaldehyde is a primary indoor pollutant, the samples were subjected to repeated adsorption tests for formaldehyde. This work focused on the samples (IN-2 and EX-2) with the best adsorption performance, and the reusability performance for formaldehyde was tested over five cycles. The process for repeated adsorption tests involved: 1) taking out the sample after adsorption of formaldehyde; 2) subjecting the samples to ultrasonic treatment in methanol solution for 10 minutes; 3) drying in an oven for 8 hours. These adsorbed formaldehyde on ZIF-8@bamboo can be easily cleaned with methanol. The samples underwent a second formaldehyde adsorption test after drying. This procedure was repeated five times to complete the full set of formaldehyde adsorption cycles. Optical photographs revealed that the samples retained intact morphology after five

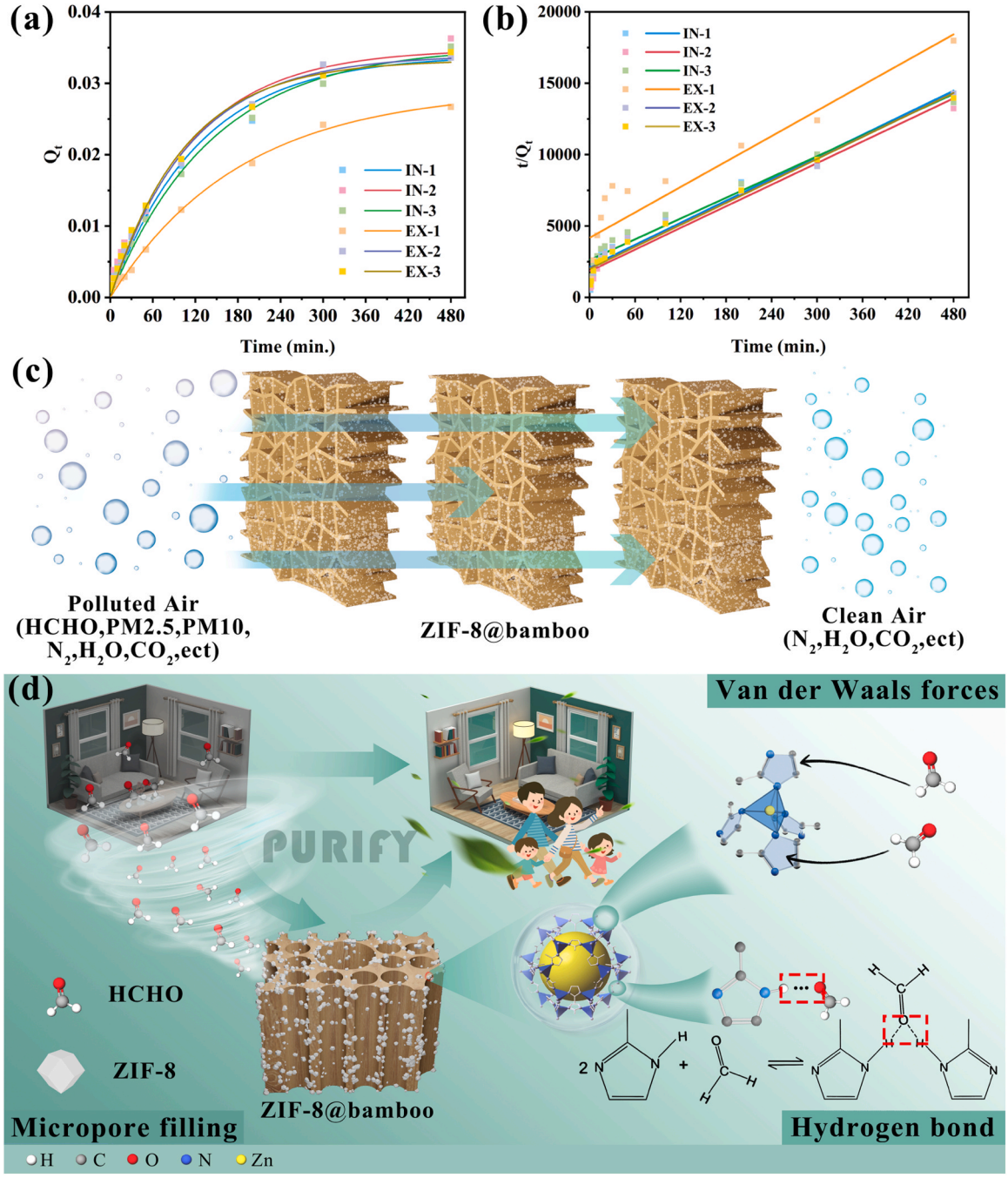


**Fig. 6.** (a) Pseudo-first-order, and (b) pseudo-second-order kinetic fitting plots for formaldehyde adsorption on different samples. (c) Schematic representation of formaldehyde adsorption efficacy. (d) The diagram of formaldehyde adsorption mechanism and application for indoor environmental management by the ZIF-8@bamboo.

adsorption-desorption cycles. Both IN-2 and EX-2 showed a gradual decreased trend in adsorption rate with each cycle but still maintained a formaldehyde degradation efficiency of 45 % (Fig. 5h). This decline was due to the slight loss or spillage of ZIF-8 crystals during the desorption process. As illustrated in Fig. 5c, the ZIF-8@bamboo still exhibited superior adsorption capacity even after multiple cycles compared to M0 (16.30 %). This indicates that ZIF-8@bamboo had great potential for formaldehyde removal in indoor environments.

### 3.7. Adsorption mechanism

Adsorption kinetics is vital factor for understanding and optimizing gas adsorption processes in environmental remediation field (Sun et al., 2024a). To explore the adsorption performance of ZIF-8@bamboo for formaldehyde, the adsorption kinetics of formaldehyde was determined using pseudo-first-order and pseudo-second-order kinetic equations (Zou et al., 2024; Huo et al., 2024):

$$\ln(Q_e - Q_t) = \ln Q_e - K_1 t \quad (3)$$

$$\frac{t}{Q_t} = \frac{t}{Q_e} + \frac{1}{K_2 Q_e^2} \quad (4)$$

where $Q_t$ represents the adsorption capacity at time t ($mg \cdot g^{-1}$); $Q_e$ represents the adsorption capacity at equilibrium ($mg \cdot g^{-1}$); $K_1$ and $K_2$ are the rate constant for the pseudo-first-order and pseudo-second-order kinetic model ($g \cdot mg^{-1} \cdot min^{-1}$), respectively.

As indicated in Fig. 6a, the adsorption rate was rapid due to abundant available sites at 60 minutes. These sites become saturated and the adsorption rate slowed down and eventually stabilized by 360 minutes. The initial higher $R^2$ value of the pseudo-first-order kinetic model followed by the superior fit of the pseudo-second-order model in later stages suggested a transition in adsorption mechanisms from physical to chemical interactions. During formaldehyde adsorption on ZIF-8@bamboo, physical diffusion dominated the rapid adsorption in the initial stage. The hierarchical pore structure of bamboo enables rapid diffusion and entrapment of formaldehyde molecules through physisorption. While subsequent chemisorption enhanced binding stability through chemical interactions. This synergistic contribution of both mechanisms significantly improved the overall adsorption capacity. However, it was found that the $R^2$ values of the pseudo-first-order kinetic model were mostly around 0.99, all higher than those of the pseudo-second-order kinetic model (Table. S2). This indicated that the formaldehyde adsorption by ZIF-8@bamboo was more consistent with the pseudo-first-order kinetic model, and primarily governed by physical adsorption. This also suggested that the ZIF-8@bamboo was a rapid, and efficient absorbent for removing indoor pollutants.

The ZIF-8@bamboo contained numerous micropores, which allowed formaldehyde gas molecules to diffuse inside and readily undergo physical adsorption (Fig. 6c). The ultra-micropore size of ZIF-8@bamboo was similar to that of low-carbon hydrocarbon gas molecules, providing an outstanding confinement space for formaldehyde molecules. Moreover, this multilayered hierarchical structure maximized host-guest interactions, and formed strong Van der Waals forces (Fig. 6d), thereby demonstrating an impressive adsorption capacity for indoor pollutants. Many imidazole rings were incorporated during the preparation of the ZIF-8@bamboo. The N atoms in the imidazole ring were highly electronegative and had a small atomic radius, but the combination with hydrogen atoms lead to electron deficient. Simultaneously, the electronegative oxygen atoms in the formaldehyde molecule formed hydrogen bonds with hydrogen atoms, which in turn firmly adsorbed the formaldehyde molecule. Therefore, a single oxygen atom in the formaldehyde molecule can form two hydrogen bonds to adsorb formaldehyde efficiently and stably (Fig. 6d).

## 4. Conclusions

In this study, a novel bamboo-based composites for indoor pollutants was successfully developed. Briefly, ZIF-8 nanoparticles were effectively loaded into the delignified bamboo substrate by in-situ and ex-situ methods to fabricate the ZIF-8@bamboo. This work addressed two critical challenges of the difficulty in recovering ZIF-8 and the limited adsorption capacity of bamboo for indoor pollutants. The novel developed ZIF-8@bamboo exhibited excellent adsorption performance for indoor pollutants, including efficient removal of formaldehyde, PM10, and PM2.5. The results indicate that the ZIF-8@bamboo had rapid adsorption kinetics and pleasurable recyclability, providing an effective strategy for indoor air purification. This study revealed that the formaldehyde adsorption of ZIF-8@bamboo was primarily due to physical adsorption. Moreover, it also showed remarkable adsorption capacity for small molecular pollutants like formaldehyde, indicating its potential as a remediation material for indoor environments. The findings of this research offer a scientific basis for the design and development of novel materials for indoor environmental remediation.

## CRediT authorship contribution statement

**Wu Dujuan:** Writing – original draft, Data curation. **Xin Ruiqi:** Writing – review & editing, Formal analysis. **Hu Lingling:** Writing – review & editing, Supervision, Resources, Methodology. **Tor Onder:** Resources, Methodology, Data curation. **Song Ye:** Formal analysis, Data curation. **Li Song:** Writing – review & editing. **Chen Meiling:** Writing – review & editing. **Zhu Wenkai:** Writing – review & editing, Supervision.

## Declaration of Competing Interest

The authors declare that they have no known competing financial interests or personal relationships that could have appeared to influence the work reported in this paper.

## Acknowledgements

This research was supported by Zhejiang Provincial Natural Science Foundation of China (Q24C160007), the Zhejiang Provincial University Student Science and Technology Innovation Activity Plan (New Seeding Talent Plan Subsidy Project, 2024R412A013), Basic Science (Natural science) Research Project in the Universities of Jiangsu Province (24KJB220008), and National Natural Science Foundation of China (32401675).

## Appendix A. Supporting information

Supplementary data associated with this article can be found in the online version at doi:10.1016/j.indcrop.2025.121102.

## Data availability

No data was used for the research described in the article.

## References

Ahmad, A., Ali, M., Al-Sehemi, A.G., Al-Ghamdi, A.A., Park, J.W., Algarni, H., Anwer, H., 2023. Carbon-integrated semiconductor photocatalysts for removal of volatile organic compounds in indoor environments. Chem. Eng. J. 452, 25. https://doi.org/10.1016/j.cej.2022.139436.

Bao, M.Z., Zhao, S.C., Tang, R.Q., Wei, J.G., Bao, Y.J., Li, N., Lin, F., Zhang, W.G., 2024. Effect of hygro-mechanical treatment combined with saturated steam on bamboo cell wall: structural, chemical, and hygroscopic properties. Ind. Crop. Prod. 219, 11. https://doi.org/10.1016/j.indcrop.2024.119085.

Baskar, A.V., Bolan, N., Hoang, S.A., Sooriyakumar, P., Kumar, M., Singh, L., Jasemizad, T., Padhye, L.P., Singh, G., Vinu, A., Sarkar, B., Kirkham, M.B., Rinklebe, J., Wang, S.S., Wang, H.L., Balasubramanian, R., Siddique, K.H.M., 2022. Recovery, regeneration and sustainable management of spent adsorbents from

wastewater treatment streams: a review. Sci. Total Environ. 822, 24. https://doi.org/10.1016/j.scitotenv.2022.153555.
Bathla, A., Kukkar, D., Heynderickx, P., Younis, S.A., Kim, K.H., 2023. Removal of gaseous formaldehyde by portable photocatalytic air purifier equipped with bimetallic Pt@Cu-$TiO_2$ filter. Chem. Eng. J., 143718 https://doi.org/10.1016/j.cej.2023.
Butt, F.S., Lewis, A., Dingwall, F., Mazlan, N.A., Radacsi, N., Fan, X., Chen, X., Yang, Y., Yang, S., Huang, Y., 2023. ZIF-8 with exceptional thermal stability: role of organic cosolvents in phase control and structure stabilization. Mater. Today Chem. 34. https://doi.org/10.1016/j.mtchem.2023.101804.
Cao, J., Pan, Y.T., Vahabi, H., Song, J.I., Song, P.A., Wang, D.Y., Yang, R.J., 2024. Zeolitic imidazolate frameworks-based flame retardants for polymeric materials. Mater. Today Chem. 37, 16. https://doi.org/10.1016/j.mtchem.2024.102015.
Chen, M., An, X., He, Y., Cai, L., Liu, R., Fei, B., 2024a. Ultra-microstructure analysis and model development of bamboo fiber cell walls. Int. J. Biol. Macromol. 280. https://doi.org/10.1016/j.ijbiomac.2024.135986.
Chen, Y., Liu, Y., Gong, X., Wang, J., 2024b. Photocatalytic degradation of chlorinated organic pollutants by ZnS@ZIF-8 composite through hydrogen peroxide generation by activating dioxygen under simulated sunlight irradiation. J. Colloid Interf. Sci. 654, 1417–1430. https://doi.org/10.1016/j.jcis.2023.10.156.
Chen, Z.L., Wang, D., Wang, X.Y., Yang, J.H., 2021. Enhanced formaldehyde sensitivity of two-dimensional mesoporous $SnO_2$ by nitrogen-doped graphene quantum dots. Rare Met 1–10. https://doi.org/10.1007/s12598-020-01636-6.
Cho, J.H., Lee, C., Hong, S.H., Jang, H.Y., Back, S., Seo, M.-G., Lee, M., Min, H.-K., Choi, Y., Jang, Y.J., Ahn, S.H., Jang, H.W., Kim, S.Y., 2023. Transition metal ion doping on ZIF-8 enhances the electrochemical CO2 reduction reaction. Adv. Mater. 35. https://doi.org/10.1002/a dma.202208224, 2208224.2208221-2208224.2208229.
Denning, S., Ahmad, A., A, Lucero, Jolie, M.Crawford, James, M.Carreon, Moises, A.Koh, Carolyn, A., 2021. Methane hydrate growth promoted by microporous zeolitic imidazolate frameworks ZIF-8 and ZIF-67 for enhanced methane storage. ACS Sustain. Chem. Eng. 9. https://doi.org/10.1021/acssuschemeng.1c01488.
Dimitroulopoulou, S., Dudzińska, M.R., Gunnarsen, L., Hgerhed, L., Maula, H., Singh, R., Toyinbo, O., Haverinen-Shaughnessy, U., 2023. Indoor air quality guidelines from across the world: an appraisal considering energy saving, health, productivity, and comfort. Environ. Int. 178, 108127. https://doi.org/10.1016/j.envint.2023.108127.
Elaouni, A., El Ouardi, M., Zbair, M., BaQais, A., Saadi, M., Ahsaine, H.A., 2022. ZIF-8 metal organic framework materials as a superb platform for the removal and photocatalytic degradation of organic pollutants: a review. RSC Adv. 12, 31801–31817. https://doi.org/10.1039/d2ra05717d.
Feng, Y., Wang, Q.Y., Xu, Z.C., He, Y., Chen, M.L., Li, Y.J., 2024. Flexural properties of moso bamboo induced by hydrothermal treatment. Ind. Crop. Prod. 222, 12. https://doi.org/10.1016/j.indcrop.2024.119720.
González-Martín, J., Kraakman, N.J.R., Pérez, C., Lebrero, R., Muoz, R., 2021. A state-of-the-art review on indoor air pollution and strategies for indoor air pollution control. Chemosphere 262, 128376. https://doi.org/10.1016/j.chemosphere.2020.128376.
Guo, Y., Wen, M., Song, S., Liu, Q., Li, G., An, T., 2022. Enhanced catalytic elimination of typical VOCs over $ZnCoO_x$ catalyst derived from in situ pyrolysis of ZnCo bimetallic zeolitic imidazolate frameworks. Appl. Catal. B Environ. 308, 121212. https://doi.org/10.1016/j.apcatb.2022.121212.
Haghighi, P., Haghighat, F., 2024. $TiO_2$-based photocatalytic oxidation process for indoor air VOCs removal: a comprehensive review. Build. Environ. 249, 17. https://doi.org/10.1016/j.buildenv.2023.111108.
He, C., Cai, M., Huang, Y., Fan, X., Zhu, M., 2024. Self-alignment of amino-functionalized $Ti_3C_2T_x$ modified with cerium-doped ZIF-8 nanocontainer towards anti-corrosive/wear and self-healing application. Compos. Part B Eng. 271. https://doi.org/10.1016/j.compositesb.2023.111144.
Hu, J., Lin, J., Yu, Y., Yu, W., Lai, C., Zhang, D., Huang, Y., 2024. Multifunctional bamboo-based fiber composites fabricated by assembling 3D network structures of bamboo and spatial distribution of silver nanoparticles. Compos. Sci. Technol. 255, 110739. https://doi.org/10.1016/j.compscitech.2024.110739.
Huo, D., Zhang, X., Wei, J., Wang, J., Zhang, Q., Yang, Q., Zhu, H., Zhang, F., Fang, G., Wu, T., 2024. Preparation and characterization of cellulose nanofibril/chitosan aerogels with high-adsorbability and sensitive indication for indoor free formaldehyde. Int. J. Biol. Macromol. 259. https://doi.org/10.1016/j.ijbiomac.2023.128891.
Jambovane, S.R., Nune, S.K., Kelly, R.T., McGrail, B.P., Wang, Z.M., Nandasiri, M.I., Katipamula, S., Trader, C., Schaef, H.T., 2016. Continuous, one-pot synthesis and post-synthetic modification of NanoMOFs using droplet nanoreactors. Sci. Rep. 6. https://doi.org/10.1038/srep36657.
Kharwar, Y.P., Gurusamy, T., Ramanujam, K., 2022. Copper-based non-precious metal catalysts derived from the in-situ and ex-situ loading of copper-bipyridine metal–organic framework on activated carbon for oxygen reduction reaction. J. Chem. Sci. 134. https://doi.org/10.1007/s12039-022-02067-9.
Kouser, S., Hezam, A., Khadri, M.J.N., Khanum, S.A., 2022. A review on zeolite imidazole frameworks: synthesis, properties, and applications. J. Porous Mater. 29. https://doi.org/10.1007/s10934-021-01184-z.
Law, C.K., Lai, J.H.K., Ma, X.D., Sze-To, G.N., 2024. Enhancing indoor air quality: examination of formaldehyde adsorption efficiency of portable air cleaner fitted with chemically-treated activated carbon filters. Build. Environ. 263. https://doi.org/10.1016/j.buildenv.2024.111823.
Lee, K., Jeon, Y., Kwon, G., Lee, S., Ko, Y., Park, J., Kim, J., You, J., 2024. Multiporous ZIF-8 carbon/cellulose composite beads: Highly efficient and scalable adsorbents for water treatment. Carbohyd. Polym. 335. https://doi.org/10.1016/j.carbpol.2024.122047.
Li, Z., Chen, M., Zhu, W., Xin, R., Yang, J., Hu, S., You, J., Ryu, D.Y., Lim, S.H., Li, S., 2024b. Advances and perspectives of composite nanoarchitectonics of nanocellulose/metal–organic frameworks for effective removal of volatile organic compounds. Coord. Chem. Rev. 520, 216124. https://doi.org/10.1016/j.ccr.2024.
Li, Y.Y., Zhang, S.J., Liu, S.H., Chen, Y.H., Luo, M.Q., Li, J.H., Xu, S., Hou, X.H., 2024a. Eco-friendly hydrophobic ZIF-8/sodium alginate monolithic adsorbent: an efficient trap for microplastics in the aqueous environment. J. Colloid Interf. Sci. 661, 259–270. https://doi.org/10.1016/j.jcis.2024.01.182.
Li, Y., Zhang, Y., Wanru, D., Yue, J., Xu, M., Shi, S.Q., 2018. Preparation and properties of pulp fibers treated with zinc oxide nanoparticles by in situ chemosynthesis. Holzforschung 72, 923–931. https://doi.org/10.1515/hf-2018-0013.
Liu, Y., Zhu, W., Li, Z., Xin, R., He, Y., Yang, J., Li, S., Chen, M., 2024. Bamboo-based cellulose nanofibers as reinforcement for polyurethane imitation wood. Ind. Crop. Prod. 210. https://doi.org/10.1016/j.indcrop.2024.118177.
Luo, K., Wang, Q., Xin, Q., Lei, Z., Hu, E., Wang, H., Liang, F., Wang, H., 2024. Uranium adsorption properties and mechanism of ZIF-8/microalgae composite adsorbent with crosslinked chitosan/tannic acid curing supported by quaternary phosphate ionic liquid. Desalination 592, 118079. https://doi.org/10.1016/j.desal.2024.
Nazir, M.A., Ullah, S., Shahid, M.U., Hossain, I., Najam, T., Ismail, M.A., Rehman, A.U., Karim, M.R., Shah, S.S.A., 2025. Zeolitic imidazolate frameworks (ZIF-8 & ZIF-67): synthesis and application for wastewater treatment. Sep. Purif. Technol. 356, 29. https://doi.org/10.1016/j.seppur.2024.129828.
Othman, J.A.S., Ilyas, R.A., Nordin, A.H., Ngadi, N., Alkbir, M.F.M., 2024. Recent advancements in bamboo nanocellulose-based bioadsorbents and their potential in wastewater applications: a review. Int. J. Biol. Macromol. 277. https://doi.org/10.1016/j.ijbiomac.2024.134451.
Qiu, Z., Gao, F., Zhang, Y., Li, J., You, Y., Lv, X., Dang, J., 2024. Advancing wastewater treatment and metal recovery: aminated ZIF-8 composite cellulose aerogel as an innovative biomass adsorbent for enhanced molybdenum ion adsorption. Sep. Purif. Technol. 338, 126478. https://doi.org/10.1016/j.seppur.2024.
Robertson, N.M., Qiu, A., Raju, S., Mccormack, M.C., Koehler, K., 2024. Cleaning indoor air—what works for respiratory health: an updated literature review and recommendations. J. Aller. CL IMM-Pract. 154, 847–860. https://doi.org/10.1016/j.jaci.2024.08.011.
Safaei, M., Foroughi, M.M., Ebrahimpoor, N., Jahani, S., Khatami, M., 2019. A review on metal–organic frameworks: synthesis and applications. Trends Anal. Chem. 118. https://doi.org/10.1016/j.trac.2019.06.007.
Shi, Y., Jiang, G., 2024. Effect of ZIF-8/nanocellulose on deodorization of bamboo-wood composite fibers. J. For. Eng. 9, 02. https://doi.org/10.13360/j.issn.2096-1359.202307005.
Shu, Y., Zhao, Y., Linghu, X., Liu, W., Shan, D., Zhang, C., Yi, R., Li, X., Wang, B., 2024. $NaGdF_4$: Yb, Er@ZIF-8/$MnO_2$ for photocatalytic removal of organic pollutants and pathogenic bacteria. EcoMat 6. https://doi.org/10.1002/eom2.12427.
Sun, C.Y., Qin, C., Wang, X.L., Yang, G.S., Shao, K.Z., Lan, Y.Q., Su, Z.M., Huang, P., Wang, C.G., Wang, E.B., 2012. Zeolitic imidazolate framework-8 as efficient pH-sensitive drug delivery vehicle. Dalton Trans. 41, 6906–6909. https://doi.org/10.1039/c2dt30357d.
Sun, Z.Q., Sun, B.W., Xue, J.J., He, J.H., Zhao, R.Z., Chen, Z.H., Sun, Z.X., Liu, H.K., Dou, S.X., 2024b. ZIF-67/ZIF-8 and its derivatives for lithium sulfur batteries. Adv. Funct. Mater. 43. https://doi.org/10.1002/adfm.202414671.
Sun, S., Vikrant, K., Verma, S., Boukhvalov, D.W., Kim, K.-H., 2024a. Diaminopropane-appended activated carbons for the adsorptive removal of gaseous formaldehyde using a portable indoor air purification unit. J. Colloid Interf. Sci. 653, 992–1005. https://doi.org/10.1016/j.jcis.2023.09.159.
Teng, D., Zheng, W., Wu, L., Murtaza, G., Meng, Z., Qiu, L., 2024. Smart manufacturing of ZIF-8 photonic crystals: catalytic formaldehyde degradation and colorful eco-friendly coatings. Chem. Eng. J. https://doi.org/10.1016/j.cej.2024.153527.
Tran, V.V., Park, D., Lee, Y.C., 2020. Indoor air pollution, related human diseases, and recent trends in the control and improvement of indoor air quality. Int. J. Environ. Res. 17. https://doi.org/10.3390/ijerph17082927.
Van Cleuvenbergen, S., Smith, Z.J., Deschaume, O., Bartic, C., Wachsmann-Hogiu, S., Verbiest, T., van der Veen, M.A., 2018. Morphology and structure of ZIF-8 during crystallisation measured by dynamic angle-resolved second harmonic scattering. Nat. Commun. 9 (3418). https://doi.org/10.1038/s41467-018-05713-4.
Wang, T., Chen, T., Ren, J., Zhou, X., Huang, C., Pan, A., Yong, Q., 2024e. Preparation of lignin microspheres and digestible substrates by deep eutectic solvent pretreatment using moso bamboo. J. For. Eng. 9, 05. https://doi.org/10.13360/j.issn.2096-1359.202401012.
Wang, X., Hu, J., Guan, H., Dai, X., Wu, M., Wang, X., 2024f. Wood-based catalytic filter decorated with ZIF-67 for highly efficient and continuous organic pollutant removal. Chem. Eng. J. 479. https://doi.org/10.1016/j.cej.2023.147580.
Wang, C., Kim, J., Malgras, V., Na, J., Lin, J., You, J., Zhang, M., Li, J., Yamauchi, Y., 2019. Metal–organic frameworks and their derived materials: emerging catalysts for a sulfate radicals-based advanced oxidation process in water purification. Small 15. https://doi.org/10.1016/j.ccr.2021.214277.
Wang, X., Li, J., Xing, J., Zhang, M., Liao, R., Wang, C., Hua, Y., Ji, H., 2024g. Novel synergistically effects of palladium-iron bimetal and manganese carbonate carrier for catalytic oxidation of formaldehyde at room temperature. J. Colloid Interf. Sci. 656, 104–115. https://doi.org/10.1016/j.jcis.2023.11.095.
Wang, Y., Lin, F., Liu, Y., Wang, X., Wang, Z., Wang, H., Xu, B., 2024h. Preparation of activated carbon from bamboo fiber bundles and its adsorption of phenol. J. For. Eng. 9, 06. https://doi.org/10.13360/j.issn.2096-1359.202402015.
Wang, S., Luo, L., Wu, A., Wang, D., Wang, L., Jiao, Y., Tian, C., 2024d. Recent advances in tailoring zeolitic imidazolate frameworks (ZIFs) and their derived materials based on hard template strategy for multifunctional applications. Coord. Chem. Rev. 498, 1.1–1.51. https://doi.org/10.1016/j.ccr.2023.215464.

Wang, G., Ren, Z.K., Zheng, L.K., Kang, Y.J., Luo, N., Qiao, Z.H., 2024a. Pulsed airstream-driven hierarchical micro-nano pore structured triboelectric nanogenerator for wireless self-powered formaldehyde sensing. Small 20, 13. https://doi.org/10.1002/smll.202406500.

Wang, L., Tang, M., Jiang, H., Dai, J., Cheng, R., Luo, B., et al., 2024b. Sustainable, efficient, and synergistic photocatalytic degradation toward organic dyes and formaldehyde gas via $Cu_2O$ NPs@wood. J. Environ. Manag. 351, 13. https://doi.org/10.1016/j.jenvman.2023.119676.

Wang, N., Zhou, X., Dong, Y.M., Zhang, Y., Liu, R., Kang, H.J., Wang, K.L., Li, J.Z., 2024c. Citral encapsulated into a zeolite imidazolate framework-67 (ZIF-67) cage via biomimetic mineralization as an efficient preservative for long-term antimildew efficacy of bamboo. Acs Sustain. Chem. Eng. 12, 15991–16000. https://doi.org/10.1021/acssuschemeng.4c05300.

Xin, R.Q., Wang, C.H., Zhang, Y.C., Peng, R.F., Li, R., Wang, J.N., Mao, Y.L., Zhu, X.F., Zhu, W.K., Kim, M., Nam, H.N., Yamauchi, Y., 2024. Efficient removal of greenhouse gases: machine learning-assisted exploration of metal–organic framework space. ACS Nano 18, 19403–19422. https://doi.org/10.1021/acsnano.4c04174.

Xing, X., Wang, Y., Zhang, Z., Wei, M., Zhang, X., Zhou, J., Sun, Z., Liu, T., 2024. $MgBu_2$ nanosheets encapsulated in ZIF-8 for producing carbon scaffold in situ nanoconfined Mg hydrogen storage materials: record-high loading and decreased dehydrogenation enthalpy. Nano. Energy 127. https://doi.org/10.1016/j.nanoen.2024.109740.

Ye, H.R., Wu, Y., Jin, X., Wu, J.M., Gan, L., Li, J.Z., Cai, L.P., Liu, C.W., Xia, C.L., 2024. Creation of wood-based hierarchical superstructures via in situ growth of ZIF-8 for enhancing mechanical strength and electromagnetic shielding performance. Adv. Sci. 11, 11. https://doi.org/10.1002/advs.202400074.

Yen, T.T., Vikrant, K., Szulejko, J.E., Kim, K.H., 2024. Uncharacteristic adsorption breakthrough behavior of a core-shell copper hydroxysulfate metal–organic framework against gaseous formaldehyde. Adv. Funct. Mater. 34, 12. https://doi.org/10.1002/adfm.202312022.

Yu, H., Zheng, H., Zhan, M., Zhang, W., Wang, J., Pan, X., Zhuang, X.W., 2020. Surface characterization and biodegradability of sodium hydroxide-treated Moso bamboo substrates. Eur. J. Wood Wood Prod. 1–9. https://doi.org/10.1007/s00107-020-01613-x.

Zhang, X.F., Wang, Z., Song, L., Yao, J., 2021. In situ growth of ZIF-8 within wood channels for water pollutants removal. Sep. Purif. Technol. 266, 118527. https://doi.org/10.1016/j.seppur.2021.118527.

Zhao, X., Ye, H., Chen, F., Wang, G., 2024. Bamboo as a substitute for plastic: research on the application performance and influencing mechanism of bamboo buttons. J. Clean. Prod. 446. https://doi.org/10.1016/j.jclepro.2024.141297.

Zhu, W., Chen, M., Jang, J., 2024. Amino-functionalized nanocellulose aerogels for the superior adsorption of $CO_2$ and separation of $CO_2/CH_4$ mixture gas. Carbohydr. Polym. 323. https://doi.org/10.1016/j.carbpol.2023.121393.

Zhu, W., Han, M., Kim, D., Zhang, Y., Kwon, G., You, J., Jia, C., Kim, J., 2022. Facile preparation of nanocellulose/Zn-MOF-based catalytic filter for water purification by oxidation process. Environ. Res. 205, 112417. https://doi.org/10.1016/j.envres.2021.112417.

Zhu, W., Han, M., Kim, D., Park, J., Choi, H., Kwon, G., You, J., Li, S., Park, T., Kim, J., 2023a. Highly catalytic and durable nanocellulose fibers-based nanoporous membrane film for efficient organic pollutant degradation. J. Water Process. Eng. 53. https://doi.org/10.1016/j.jwpe.2023.103620.

Zhu, W.K., Kim, D., Han, M.S., Jang, J., Choi, H., Kwon, G., Jeon, Y., Ryu, D., Lim, S.H., You, J.M., Li, S., Kim, J., 2023b. Fibrous cellulose nanoarchitectonics on N-doped Carbon-based Metal-Free catalytic nanofilter for highly efficient advanced oxidation process. Chem. Eng. J. 460, 12. https://doi.org/10.1016/j.cej.2023.141593.

Zou, J., Tang, X., He, L., Jin, W., Yu, Q., Yu, J., Sun, L., Cai, G., Wang, X., Cheng, D., 2024. Metal–organic framework derived N-doped zinc oxide carbon nanocomposites for catalytic removal of dye and formaldehyde. Polym. Compos. 45. https://doi.org/10.1002/pc.27833.